The asymmetric clock model on a Cayley tree

1984 J. Phys. A: Math. Gen. 17 1493

(http://iopscience.iop.org/0305-4470/17/7/017)

J. Phys. A: Math. Gen. **17** (1984) 1493–1507. Printed in Great Britain

The asymmetric clock model on a Cayley tree

K Fesser†§ and H J Herrmann‡

† Theoretical Division, Los Alamos National Laboratory, Los Alamos, NM 87545, USA
‡ Service de Physique Théorique, CEN Saclay, 91191 Gif-sur-Yvette Cedex, France

Received 28 November 1983

Abstract. The asymmetric clock model is studied on a Cayley tree and commensurate and incommensurate phases are found. The transition lines are obtained from stability conditions and characteristic points in the phase diagram are analysed by numerical iteration. A critical endpoint is found for the case of three states per site and a Lifshitz point for the case of four states per site.

1. Introduction

Simple models with commensurate and incommensurate modulated phases have been proposed and studied in the last years, the best known of which being the ANNNI model (Elliott 1961, Selke and Fisher 1979, Selke 1983). The asymmetric p-state clock model—also called chiral model—was introduced by Ostlund (1981) and Huse (1981). Every site can be in one of p different states. In this respect it is more complex than the ANNNI model. It exhibits modulated phases if the number p of possible states on one site is larger than two. On the other hand it has only nearest-neighbour interactions, while in the ANNNI model one has competing nearest- and next-nearest-neighbour interactions. The asymmetric clock model is similar to models studied by Cardy (1982), Kardar (1982) and Kardar and Berker (1982).

The p-state asymmetric clock model can be described as follows: on each site of the lattice put a state $\sigma_i \in \{1, \ldots, p\}$ and let the interaction be defined by the Hamiltonian

$$\mathcal{H} = -J \sum_{\langle i,j \rangle_\parallel} \cos\left(\frac{2\pi}{p}(\sigma_i - \sigma_j - \Delta)\right) - J \sum_{\langle i,j \rangle_\perp} \cos\left(\frac{2\pi}{p}(\sigma_i - \sigma_j)\right) \tag{1}$$

where the first sum is over nearest neighbours in one given direction $\boldsymbol{n}$ while the second sum is over nearest neighbours in all directions perpendicular to $\boldsymbol{n}$. The real number Δ is an additional parameter of the model.

In two dimensions this model has been studied by Ostlund (1981) in the free fermion approximation, with Monte Carlo simulations by Selke and Yeomans (1982), with series expansion by Barber (1982) and with Migdal renormalisation by Huse (1981). In two dimensions one finds p different ordered low-temperature phases and, between these and the paramagnetic phase, a so-called modulated phase which has similar properties as the weak phase of the XY model. In this phase the magnetisation

§ Present address: Physikalisches Institut, Universität Bayreuth, 8580 Bayreuth, Federal Republic of Germany.

0305-4470/84/071493+15$02.25

is characterised by a continuously varying wavevector q in the $\boldsymbol{n}$ direction while in the ordered phases q is zero (ferromagnetic phase) or $1/p$ (helical phases). For $p>5$ the ordered and the paramagnetic phases are completely separated by the modulated phase, for $p=4$ the ordered and paramagnetic phases touch each other only at integer values of Δ and for $p=3$ there is a whole line of values of Δ according to Ostlund (1981) limited by Lifshitz points—at which ordered and paramagnetic phases touch.

If the dimension is greater than two (Yeomans and Fisher 1981, Huse 1981) or in mean field approximation (Öttinger 1982, 1983) no modulated phase is present. Instead, one finds an infinite set of ordered commensurate phases with the values of q varying like a devil's staircase with Δ (Aubry 1978).

Here we study a similar p-state asymmetric clock model on a Cayley tree by considering only the first sum in (1) as our Hamiltonian. In other words, $\boldsymbol{n}$ simply points towards the centre of the tree and the modulation of a phase would take place with respect to the generation of the tree. A similar approach has been made by Vannimenus (1981) for the ANNNI model. We also expect to find commensurate and incommensurate phases and the behaviour should be more similar to that of Hamiltonian (1) on a low-dimensional lattice than on a high-dimensional one because in the latter case the second sum of (1) becomes more and more important.

On the Cayley tree the model is solved easily by a recursion relation which we present in § 2. This recursion relation which can be viewed as nonlinear map is iterated numerically in § 3 and different types of attractors characterise the different phases. In §§ 4 and 5 we use stability considerations to calculate the transition lines between the paramagnetic and modulated phases and between the ferromagnetic and modulated phases. Using the Fourier transform of the magnetisation we analyse in § 6 the modulated phase in more detail. The peculiar behaviour around the point at which the three phases meet is investigated in § 7 and the results are summarised in § 8.

2. Model and symmetries

We shall consider the p-state asymmetric clock model on a Cayley tree of branching ratio k. The case $k=3$ is illustrated in figure 1. On every vertex on the tree we place the variable σ_l which can take the values $1,\ldots,p$. The Hamiltonian is

$$\mathcal{H}=-J\sum_{\langle l,m\rangle}\cos\left(\frac{2\pi}{p}(\sigma_l-\sigma_m-\Delta)\right) \tag{2}$$

with the sum running over all nearest neighbours. On the boundary of the tree—which we call the zeroth generation—we fix the state to be 1 on all sites (see figure 1). Now the partition function is calculated iteratively by moving from the boundary towards the interior of the tree. The partial partition function of a branch of n generations where the innermost site is in state i is denoted by $Z_n(i)$. Then one can calculate the partial partition function of the next generation by

$$Z_{n+1}(i)=(\omega_{i1}Z_n(1)+\ldots+\omega_{ip}Z_n(p))^k \tag{3}$$

for all $i=1,\ldots,p$ with $(\beta=1/k_BT)$

$$\omega_{ij}=\exp(\beta J\cos(2\pi/p)(i-j-\Delta)),\qquad i,j=1,\ldots,p. \tag{4}$$

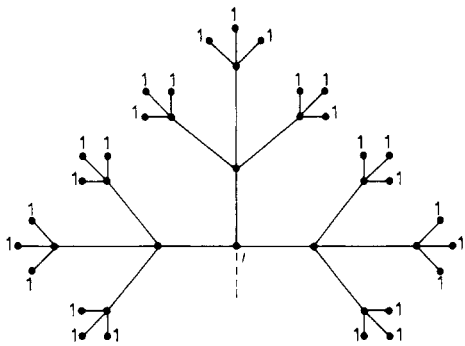

Figure 1. Branch of a Cayley tree of branching ratio $k=3$ in its third generation. The partial partition function is $Z_3(i)$.

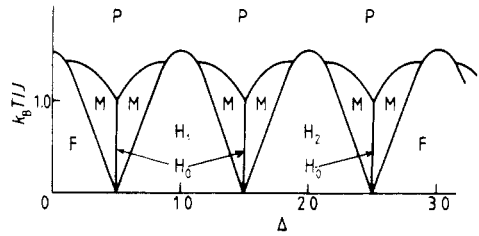

Figure 2. Complete phase diagram for $p=3$, $k=2$ illustrating the symmetries discussed in § 2. P: paramagnetic phase, M: modulated phase, F: ferromagnetic phase, H_1 and H_2 are the two helical phases of period 3, H_0 is the helical phase of period 6.

Equation (3) is a recursion relation where the first step is given by the boundary condition:

$$Z_1(i) = \exp(\beta J \cos(2\pi/p)(i-1-\Delta)). \tag{5}$$

The matrix $(\omega_{i,j})$ has the symmetries

$$\omega_{i,j}(\Delta) = \omega_{(i+1) \bmod p,j}(\Delta-1) = \omega_{i,(j+1) \bmod p}(\Delta+1) \tag{6}$$

and

$$\omega_{i,j}(\Delta) = \omega_{j,i}(-\Delta) \tag{7}$$

for all $i, j = 1, \ldots, p$. Since we have from (6)

$$\omega_{i,j} = \omega_{(i-1) \bmod p,(j+1) \bmod p}(\Delta) \tag{8}$$

we define for later use

$$\Omega_i = \omega_{i,1}(\Delta). \tag{9}$$

The case $\Delta = 0$ is the usual p-state vector Potts model the behaviour of which is well understood. For $p=2$ and $n=3$ it is the same as the p-state standard Potts model. This has been studied on a Cayley tree by Baumgärtel and Müller-Hartmann (1982) and by Moraal (1981, 1982). For $p=3$, it has a first-order phase transition between a ferromagnetic and a paramagnetic phase.

For a general Δ one obtains a phase diagram of the type shown in figure 2 for $p=3$ and $k=3$. It repeats itself identically if one adds to Δ a multiple of p as a consequence of the symmetry (6). One can see that for a certain range of values of Δ an intermediate (modulated) phase appears between the ordered and disordered phases. The ordered phases are ferromagnetic ($\langle 111 \rangle$) or helical ($\langle 123 \rangle$ and $\langle 132 \rangle$ for $p=3$). It is sufficient to calculate the phase boundaries and their properties for $\Delta \in [0, \frac{1}{2}]$ only, since due to the symmetries (6) and (7) one can obtain the rest of the phase diagram by permutations of the states if one goes from one generation of the tree to the next. Therefore, we will subsequently show diagrams for $0 \leqslant \Delta \leqslant 1$ only.

The ordered phase order parameter is usually the magnetisation. In p-state models $p-1$ different magnetisations can be defined. As we are going to study modulated

phases the magnetisation will be space dependent, i.e. dependent on the generation of the tree. We define

$$M_i(n) = Z_n(i) \Big/ \sum_{j=1}^{p} Z_n(j), \qquad i = 1, \ldots, p. \tag{10}$$

Clearly one of these p quantities is a function of the others through

$$\sum_{i=1}^{p} M_i(n) = 1 \tag{11}$$

but any choice of $p-1$ of the quantities defined in (10) is a good set of independent magnetisations. In the forthcoming discussion we will also use a mean magnetisation

$$M(n) = \sum_{i=1}^{p} iM_i(n). \tag{12}$$

In the modulated phase all magnetisations defined above will vary periodically with n (in general with a complicated period). A good order parameter of the modulated phase is, therefore, the wavevector q of the function $M(n)$ from equation (12). Obviously for the ferromagnetic phase we have $q = 0$ and for the helical phases $q = 2\pi/p$. If the limit of infinite iterations is well defined we will use the nomenclature $M_i = \lim_{n\to\infty} M_i(n)$ and $M = \lim_{n\to\infty} M(n)$.

3. The nonlinear map

For given n let us define the quantities

$$x_i = Z_n(i+1)/Z_n(1), \qquad x_i' = Z_{n+1}(i+1)/Z_{n+1}(1) \tag{13}$$

for all $i = 1, \ldots, p-1$. Then we obtain from equations (3) and (9) the expression

$$\begin{aligned} x_1' &= \left(\frac{\Omega_p + \Omega_1 x_1 + \ldots + \Omega_{p-1} x_{p-1}}{\Omega_1 + \Omega_2 x_1 + \ldots + \Omega_p x_{p-1}}\right)^k \\ &\vdots \\ x_{p-1}' &= \left(\frac{\Omega_2 + \Omega_3 x_1 + \ldots + \Omega_1 x_{p-1}}{\Omega_1 + \Omega_2 x_1 + \ldots + \Omega_p x_{p-1}}\right)^k \end{aligned} \tag{14}$$

which defines a nonlinear $(p-1)$ dimensional map $F: \boldsymbol{x} \to \boldsymbol{x}'$. For fixed temperature T and branching ratio k, the asymmetry Δ serves as a control parameter. The different phases of the model (2) are now characterised by the different fixed points and limit cycles of the map F of equation (14). The phase boundaries are given by the limits of stability of the fixed points under the transformation F. The criterion of stability of a phase is given by $|\lambda_j| < 1$ for all $j = 1, \ldots, p-1$ where λ_j are the eigenvalues of the Jacobian

$$J_{ik} = \partial F_i / \partial x_k, \qquad i, k = 1, \ldots, p-1 \tag{15}$$

at the fixed point $\boldsymbol{x}^{\mathrm{FP}}$ of F that characterises this phase ($\boldsymbol{x}^{\mathrm{FP}} = F(\boldsymbol{x}^{\mathrm{FP}})$).

The map F of equation (14) has the property that the determinant of the Jacobian is less than 1: $|\det J_{ik}| < 1$ and hence the fixed points and limit cycles described below are attracting. This is in contrast to the nonlinear maps which arise in mean field theory of similar models. These maps are area preserving (Hamiltonian), i.e. $|\det J_{ik}| = 1$ (cf Bak 1981, Jensen and Bak 1983, Öttinger 1983).

There is one trivial fixed point $x_1 = \ldots = x_{p-1} = 1$ which characterises the paramagnetic phase. The corresponding partial magnetisations are all equal, $M_i = 1/p$, and the mean magnetisation takes the value $M = (p+1)/2$. In figure 3 the behaviour of the map F is illustrated for the iteration towards this fixed point for the case $p = 3$, $k = 2$, $k_B T/J = 0.3$ and $\Delta = 0.489$; figure 3(a) shows a plot of $x_1(n+1)$ against $x_1(n)$ which is a 'phase portrait' of the dynamical variable x or Z respectively. This kind of analysis is well known from dynamical systems theory (see e.g. Helleman 1980). Since we have chosen the parameters for this figure in the paramagnetic phase close to the modulated phase the points $x_1(n)$ spiral towards the fixed point $x_1(n \to \infty) = 1$. Correspondingly the mean magnetisation as defined in equation (12) converges towards its asymptotic value $M = 2.0$ with oscillations with decreasing amplitude. This transient behaviour reminiscent of the modulated phase disappears more quickly the further we move with our parameters into the paramagnetic phase.

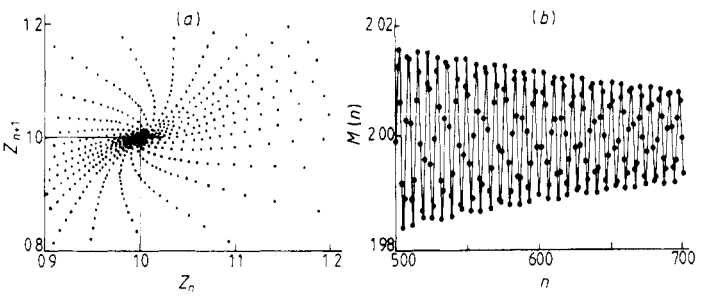

Figure 3. (a) Plot of the $(n+1)$th iterate of the partition function as the nth iterate for the case $p = 3$, $k = 2$, $k_B T/J = 0.3$ and $\Delta = 0.489$. (b) Mean magnetisation (dots) defined in equation (12) as a function of the generation of the tree for the parameter as in (a).

As a representative for the behaviour of the Hamiltonian of equation (2) we show all qualitatively different cases for the special values $p = 3$, $k = 3$ and $k_B T/J = 0.8$ in figure 4, i.e. making a horizontal cut through the phase diagram of figure 2. We chose the number n of iterations to be large enough to exclude boundary effects as discussed in the previous paragraph. Figure 4(a) is at $\Delta = 0.1$ and shows the ferromagnetic fixed point and the corresponding constant magnetisation. This fixed point bifurcates into a limit cycle which can be seen in figure 4(b) for $\Delta = 0.4$; the mean magnetisation shows an oscillatory behaviour $M(n) \sim \cos q \cdot n +$ higher harmonics. This limit cycle

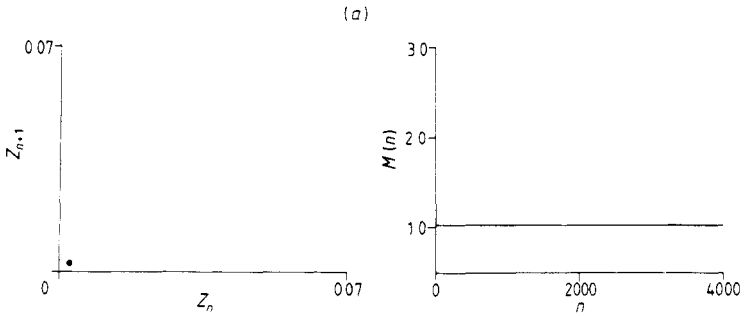

Figure 4.

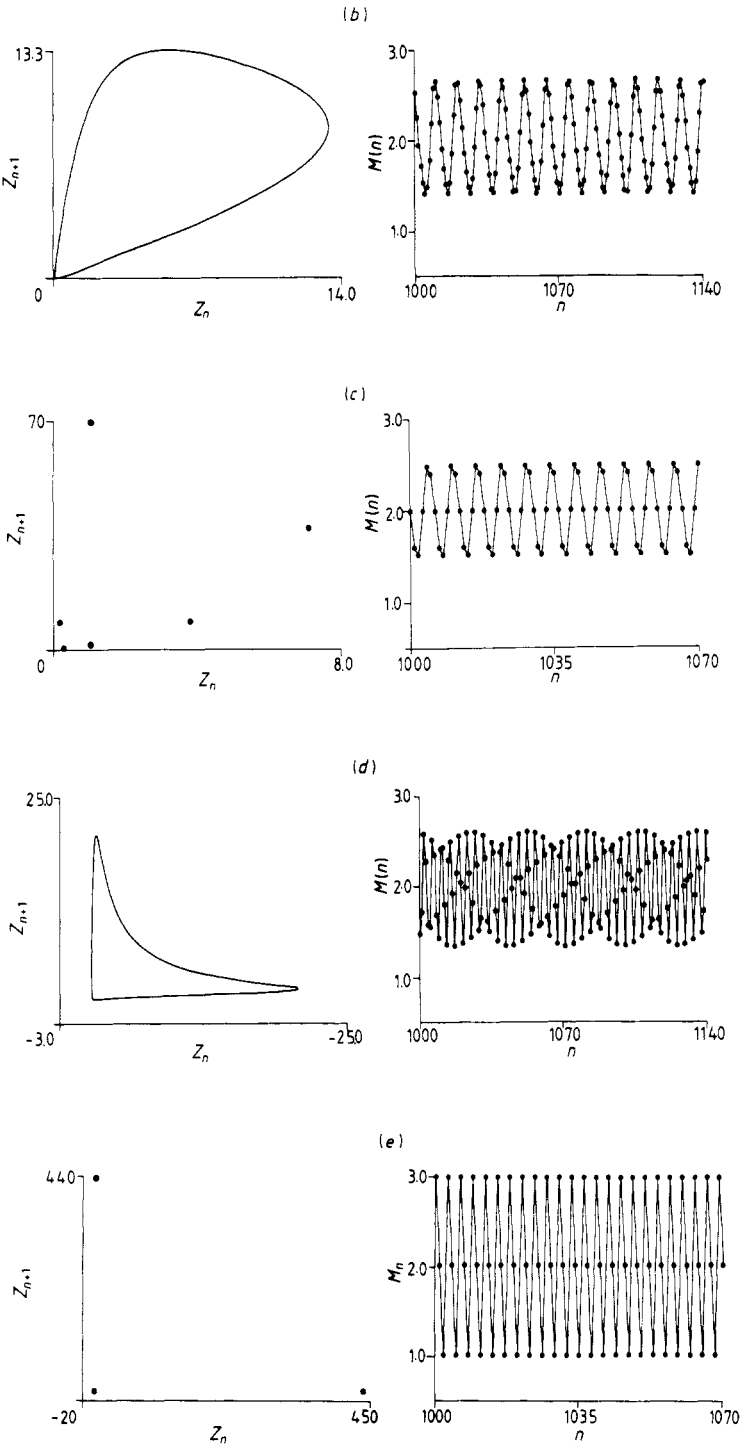

Figure 4. Plots as in figure 3 of the partition function (left) and magnetisation (right) for $p=3$, $k=3$, $k_BT/J=0.8$ for different values of Δ: (*a*) 0.1, (*b*) 0.4, (*c*) 0.5, (*d*) 0.6, (*e*) 0.9. n is chosen large enough to exclude boundary effects.

(or the wavevector q) characterises the modulated phase. For $\Delta = 0.5$ (figure 4(c)) we have the special case of $2p$ fixed points and hence a mean magnetisation oscillating exactly with a period $2p$ or wavevector $q/2\pi = 1/2p$. This is stable only for $\Delta = 0.5$; for Δ slightly less or larger than $\Delta = 0.5$ we have limit cycle behaviour. Figure 4(d) shows the modulated phase for $\Delta = 0.6$. Here the limit cycle has a different shape and the oscillation of M is characterised by an additional second, smaller wavevector compared to the case of figure 4(b). Finally, for $\Delta = 0.9$ we have p fixed points characterising one of the helical phases (figure 4(e)).

The complete phase diagrams for $p = 2, 3, 4$ and 5 are shown in figure 5. The different phase boundaries and the modulated phases will be discussed later in detail. We want to conclude this section with the remark that by varying Δ (or T) we found bifurcations from one fixed point to a limit cycle to p (or $2p$) fixed points and back, but no chaotic behaviour, i.e. strange attractors, which would be a hint for a glass phase. We want to point out that the bifurcations by varying Δ or T are of different type: the transition modulated-ferro (variation of Δ) is produced by a slowing down of the speed ($\mathrm{d}/\mathrm{d}n$) of the iteration on the limit cycle until it 'freezes' in (ferromagnetic fixed point). The modulated-para bifurcation (variation of T) on the other hand is given by a continuous shrinking of the area of the limit cycle to one point (paramagnetic fixed point).

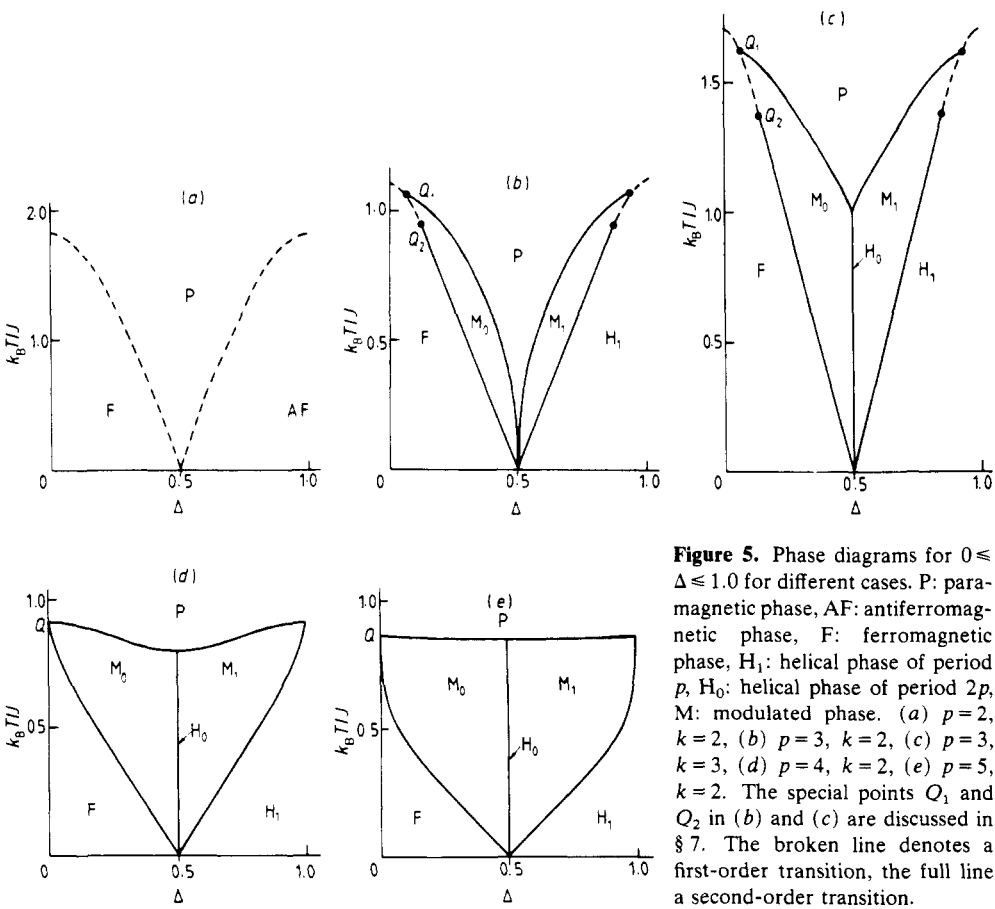

Figure 5. Phase diagrams for $0 \leqslant \Delta \leqslant 1.0$ for different cases. P: paramagnetic phase, AF: antiferromagnetic phase, F: ferromagnetic phase, H_1: helical phase of period p, H_0: helical phase of period $2p$, M: modulated phase. (a) $p = 2$, $k = 2$, (b) $p = 3$, $k = 2$, (c) $p = 3$, $k = 3$, (d) $p = 4$, $k = 2$, (e) $p = 5$, $k = 2$. The special points Q_1 and Q_2 in (b) and (c) are discussed in § 7. The broken line denotes a first-order transition, the full line a second-order transition.

4. The stability of the paramagnetic phase

We will now discuss the calculation of the phase transition line between the paramagnetic phase and the other phases by means of a stability analysis. This analysis is close to that performed by Vannimenus (1981) for the ANNNI model. As already mentioned in the preceding section the paramagnetic fixed point is $x_1 = \ldots = x_{p-1} = 1$. The stability criterion (15) yields as condition for the phase boundary

$$k\lambda = \sum_{i=1}^{p} \Omega_i \tag{16}$$

with $\lambda = \max_j |\lambda_j|$ and λ_j being the eigenvalues of the matrix

$$\begin{pmatrix} (\Omega_1-\Omega_2)(\Omega_2-\Omega_3)\ldots(\Omega_{p-1}-\Omega_p) & & \\ (\Omega_p-\Omega_2) & & \\ \vdots & & \\ (\Omega_3-\Omega_2) & \ldots & (\Omega_1-\Omega_p) \end{pmatrix}. \tag{17}$$

The eigenvalue λ_j is real if the instability occurs at the transition to the ferromagnetic phase and complex for the transition to the modulated phase. The lines of limits of stability defined by equation (16) are transition lines if there are no other fixed points of the map F of equation (14) which are stable on this line or if the other fixed points have their limit of stability on the same line. The first is the case for the transitions paramagnetic–modulated, the latter occurs for $p = 2$. If, however, there is a region of T and Δ where two fixed points of the map F are stable simultaneously the present analysis is not sufficient to determine which one actually corresponds to the minimum of the free energy. This is the case at the transition paramagnetic–ferromagnetic (or helical) for $p = 3$. We then determine the physical phase by iteration of the map F of equation (14) as described in the preceding section.

We shall now discuss in detail the transition lines out of the paramagnetic phase for different p. Figure 5(a) shows the Ising case $p = 2$ for $k = 2$. Here we have no modulated phase and the phase boundary can be calculated very easily. We obtain

$$k_B T_c/J = \frac{2}{\ln[(k+1)/(k-1)]} \cos \pi\Delta \qquad \text{for } 0 \leqslant \Delta \leqslant \tfrac{1}{2} \tag{18}$$

which is the same result as for the stability of the ferromagnetic phase.

The phase diagram for $p = 3$ and $k = 2$ is shown in figure 5(b). The stability criterion (16) yields an implicit equation for the transition line:

$$2\cosh\left(\frac{\sqrt{3}}{4}\frac{J}{k_B T_c}\sin\frac{2\pi}{3}\Delta\right) = \exp\left(\frac{3}{4}\frac{J}{k_B T_c}\cos\frac{2\pi}{3}\Delta\right) \qquad \text{for } 0 \leqslant \Delta \leqslant \tfrac{1}{2} \tag{19}$$

and for special cases we calculate the transition temperature for arbitrary k:

$$k_B T_c/J = 3/[2\ln((k+2)/(k-1))] \qquad \text{for } \Delta = 0 \tag{20}$$

and

$$k_B T_c/J = 3/[(2\ln((k+1)/(k-2))] \qquad \text{for } \Delta = \tfrac{1}{2}. \tag{21}$$

As can be seen from (21) the paramagnetic phase touches the zero temperature line

at $\Delta = \frac{1}{2}$ (for $k = 2$) and has the behaviour

$$k_B T_c / J = -3/(4 \ln|\tfrac{1}{2} - \Delta|) \tag{22}$$

in the vicinity of this point. For all other values of k the RHS of equation (21) is finite so that only in the Ising case or for $p = 3$ and $k = 2$ have we the possibility of a paramagnetic phase at $T = 0$ (see figure 5(*c*) for $p = 3$ and $k = 3$).

The phase diagrams for $p = 4$ and $p = 5$ (for $k = 2$) are shown in figures 5(*d*) and 5(*e*), respectively. The paramagnetic transition line flattens with increasing p and for $p \to \infty$ one expects no curvature at all. At $\Delta = 0$ the transition temperature for $p = 4$ is given by

$$k \sinh(J/k_B T_c) = 1 + \cosh(J/k_B T_c) \tag{23}$$

which in the special case $k = 2$ yields $k_B T_c / J = 1/\ln 3 = 0.9012$. For $p = 5$ and $k = 2$ the value at $\Delta = 0$ is numerically $k_B T_c / J = 0.8712$ and for $p = 10$ we get $k_B T_c / J = 0.8636$. (Both are obtained from 10 000 iterations of the map F.)

5. The stability of the ferromagnetic phase

The stability analysis for the ferromagnetic phase is more complicated than the analysis for the paramagnetic phase shown in § 4 because the fixed point is not the same for the whole phase but depends on T and Δ. In consequence one has to obtain in addition the values of the relative magnetisations

$$A_i = \lim_{n \to \infty} (Z_n(i+1)/Z_n(1)) = M_{i+1}/M_1, \qquad i = 1, \ldots, p-1. \tag{24}$$

One can actually calculate the limit of the stability region by inverting the process by giving a set of values $\{A_i\}$ and calculating its corresponding values of T and Δ and the eigenvalue λ of the Jacobian at this point. As in § 4 the condition $|\lambda| < 1$ is the condition for stability. This inverting procedure can be formulated for any p but for $p > 3$ it involves a higher-dimensional Newton algorithm and is thus numerically more tedious. Therefore we will present here the detailed prescription for $p = 3$ and show results for this case only.

The prescription to find one point of the limiting line of stability in the (T, Δ) plane is the following. Choose a fixed value for A_1 and start with a tentative value for A_2. Calculate α_1 and α_2 from the coupled linear equations

$$\begin{aligned} A_1^{1/k} \gamma_0 &= \gamma_1, \\ A_2^{1/k} \gamma_0 &= \gamma_2, \end{aligned} \tag{25}$$

with

$$\gamma_0 = 1 + \alpha_1 A_1 + \alpha_2 A_2, \qquad \gamma_1 = A_1 + \alpha_1 A_2 + \alpha_2, \qquad \gamma_2 = A_2 + \alpha_1 + \alpha_2 A_1. \tag{26}$$

Then calculate the eigenvalues λ_i of the stability matrix

$$\begin{pmatrix} A_1(\gamma_1^{-1} - \alpha_1 \gamma_0^{-1}) & A_1(\alpha_1 \gamma_1^{-1} - \alpha_2 \gamma_0^{-1}) \\ A_2(\alpha_2 \gamma_2^{-1} - \alpha_1 \gamma_0^{-1}) & A_2(\gamma_2^{-1} - \alpha_2 \gamma_0^{-1}) \end{pmatrix}. \tag{27}$$

Now look for that value of A_2 (by a Newton algorithm) so that

$$k\lambda = 1$$

where $\lambda = \max_i |\lambda_i|$. The pair (A_1, A_2) determines the magnetisations of a fixed point on the limiting line of stability of the (T, Δ) plane. The corresponding values for T and Δ are obtained from the α_1 and α_2 by

$$\ln \alpha_i = \frac{J}{k_B T}\left(\cos\frac{2\pi}{3}(\Delta + i) - \cos\frac{2\pi}{3}\Delta\right), \qquad i = 1, 2. \tag{28}$$

The proof of the above procedure is done in a straightforward way. These values A_1 and A_2 yield together with $M_1 + M_2 + M_3 = 1$ the three magnetisations on the whole stability line. This is shown in figure 6 for the case $p = 3$, $k = 3$. It should be noted that M_3 is not zero at $\Delta = 0.5$ as perhaps suggested by the figure but has a finite but small value. Furthermore, we remark that M_2 has a maximum at about $\Delta = 0.02$. These qualitative features are also found for other values of k.

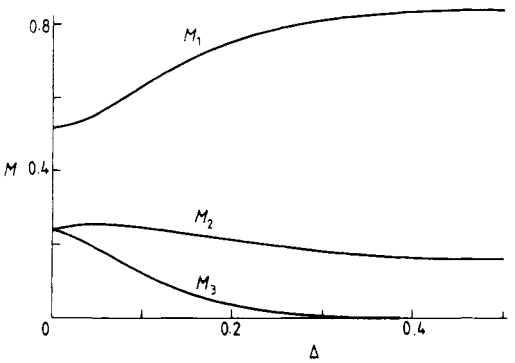

Figure 6. Partial magnetisations as a function of the asymmetry Δ along the ferromagnetic transition line for $p = 3$ and $k = 3$.

The stability lines in the (T, Δ) plane are shown in the phase diagrams of figure 5 for different values of p and k. The lines are partly first order and partly second order. This will be discussed in § 6. For $p > 4$ this stability line is not obtained by the procedure described above, but simply by iterating the map F (equation (14)).

Except for the case $p = 2$ where the stability lines for the ferromagnetic phase and the paramagnetic phase coincide there is one special point in the phase diagrams in which both lines meet. The nature of this point will be investigated in § 7. For $p > 4$ this occurs at $\Delta = 0$ and the ferromagnetic line is always below the paramagnetic line for other values of Δ. Note that in contrast to Ostlund (1981) there is no modulated phase at $\Delta = 0$ separating the ferro- and paramagnetic phases. For $p = 3$, however, the two stability lines cross at a finite value of $\Delta = \Delta_0$ and for values $0 < \Delta < \Delta_0$ there is a region where both phases are 'stable' in the sense defined in § 3. The question of which one of these phases is *thermodynamically stable* or *metastable* cannot be decided by this criterion. We have settled this question in this case by iterating equation (14) and found that in this region the ferromagnetic phase is the stable one. Thus in the phase diagrams of figure 5 the paramagnetic stability line is not plotted in this region. The fact that we found a metastable and a stable phase also shows us that the transition is of first order as marked in the diagrams of figure 5 by broken lines.

6. The modulated phase

As already mentioned in § 3, the order parameter for the modulated phase is the wavevector of the oscillating mean magnetisation $M(n)$. This wavevector is obtained easily by a Fourier transform of the magnetisation $M(n)$. For this purpose we have used the standard fast Fourier transform algorithm. Due to the finite number of iterations we are not able to resolve values of q which are smaller than 0.003. A typical example is given in figure 8(b) for $p=3$, $k=3$, $k_BT/J=0.8$ and $\Delta=0.4$. ($S(q)=|N^{-1}\Sigma_{n=n_0}^{n_0+N} M(n)\exp(-iqn)|^2$.) We find not only a peak at $q=0.57$ indicating a period $2\pi/q=11.0$ but also peaks at higher harmonics of this fundamental wavevector due to the nonlinearity of the map F of equation (14).

By changing Δ at fixed T we find that the wavevector q varies *continuously* with Δ. This result is in contrast to similar models (Öttinger 1982, 1983, Huse 1981) in mean field theory where one finds instead an infinite set of ordered commensurate phases with the values of q varying like a devil's staircase. The reason for this difference lies in the fact that on a Cayley tree the asymmetry parameter acts on all directions and hence the model behaves more like a low-dimensional one while in mean field theory one has infinite dimensions without Δ and only one with the asymmetry.

At the transition to the ferromagnetic phase the wavevector vanishes at a fixed temperature as

$$q \sim (\Delta - \Delta_c(T))^{\zeta} \tag{29}$$

(except for $T > T^*$ at $p=3$, where the transition is of first order (see figure 5(c) and next section)). Figure 7(a) shows an example for this behaviour for $p=3$, $k=3$ and $k_BT/J=0.8$ ($\Delta_c(T)$ is the critical Δ at this temperature). In this case the exponent ζ is determined as $\zeta=0.526$. This exponent is not universal but depends on T: for $k_BT/J=1.2$ we obtain $\zeta=0.546$ as shown in figure 7(b). The fact that ζ varies continuously has not been found before in these models and might be related to the special nature of Cayley trees as found already for the Ising model (Müller-Hartmann and Zittartz 1974).

If we move very close to the transition line, we have to iterate the map F often enough in order to see the periodic structure of the magnetisation in the modulated phase. Figure 8(a) shows an example for $p=3$, $k=3$, $k_BT/J=1.0$ and $\Delta=0.241\,64$. Only after 24 000 iterations we can see a period of roughly 21 400. Another striking

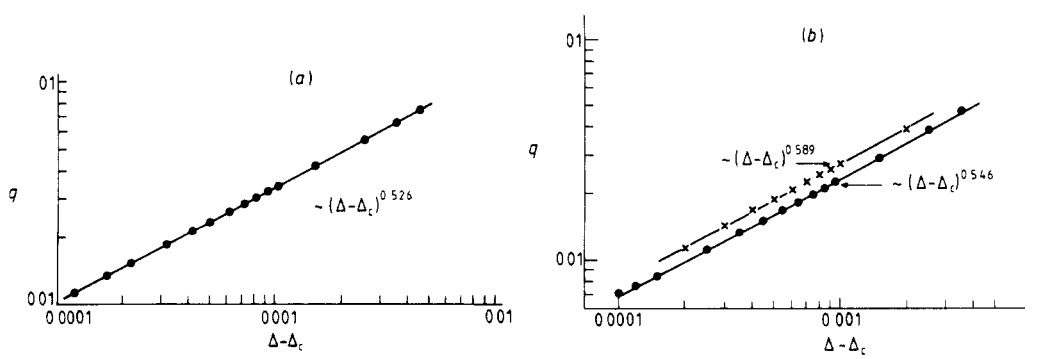

Figure 7. Log–log plot of the wavevector q in the modulated phase close to the ferromagnetic transition for $p=3$, $k=3$ and (a) $k_BT/J=0.8$, (b) $k_BT/J=1.2$ (full circles) and $k_BT/J=1.38$ (crosses).

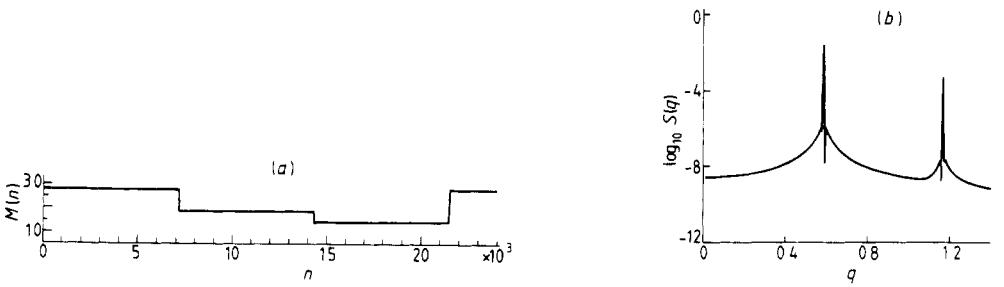

Figure 8. (*a*) Mean magnetisation as a function of generation in the modulated phase close to the ferromagnetic transition for $p=3$, $k=3$, $k_BT/J=1.0$ and $\Delta=0.241\,64$. Note the long period of ~21 400. (*b*) Typical example of the Fourier transform of the mean magnetisation ($p=3$, $k=3$, $k_BT/J=0.8$, $\Delta=0.4$).

feature is the fact that the magnetisation is constant for many iterations (i.e. a large portion of the tree) interrupted only by a few kinks connecting two of the three possible states. (This is true also for other values of p). The transition to the ferromagnetic phase can now be understood as a melting of the kink lattice where the distance between two successive kinks becomes infinite (cf Jensen and Bak 1983).

The transition from the modulated to the paramagnetic phase is characterised not by the wavevector but by the amplitude of the modulation of the magnetisation. This amplitude is correlated with the area of the limit cycle (cf § 3). In figure 9 we show the amplitude

$$dy=\max(M(n))-\min(M(n)) \tag{30}$$

if one approaches the paramagnetic-modulated transition line from the modulated phase for $p=3$, $k=3$ for Δ fixed close to Q_1 (at $\Delta=0.08$). Since this amplitude goes continuously to zero at the transition line, this transition is of second order. Since figure 9 is a log–log plot we can estimate from the slope the exponent for dy to be 0.52. This exponent changes drastically if one changes Δ and for $\Delta=0.2$ ($p=3$, $q=3$) one finds a value of 6.5. The wavevector, on the other hand, remains finite at the transition for all Δ.

7. The Lifshitz point

Here we focus on the properties of the exceptional points Q_1 and Q_2 in figures 5(*b*) and 5(*c*), for the case $p=3$ and Q for the case $p>3$. As we have seen in § 6 the question arises whether the point Q_1 is a Lifshitz point (Hornreich *et al* 1975, Michelson 1977), i.e. if q goes to zero at this point, similarly to the lower part of the ferro-modulated transition line. While for the latter we had fixed the temperature T and varied Δ only we now vary both asymmetry and temperature, so that we move on a straight line into the point Q_1. (The result does not depend on the slope of this line.) Surprisingly we find that q does not vanish when we approach Q_1 but remains finite even with $|\Delta-\Delta_c|<10^{-6}$ whereas in the former case we found that q vanished already for $|\Delta-\Delta_c|<10^{-4}$ (see figure 10), where Δ_c is the critical asymmetry at which the transition modulated to ferromagnetic phase occurs. This is thus a jump in q at Q_1,

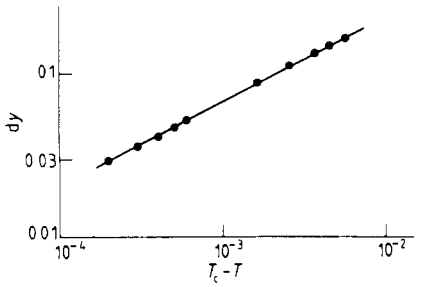

Figure 9. Log–log plot of dy against $T_c - T$ at fixed $\Delta = 0.08$ for $p = 3$, $k = 3$. $T_c = 1.6156$ is the critical temperature of the paramagnetic-modulated phase. The slope is 0.52.

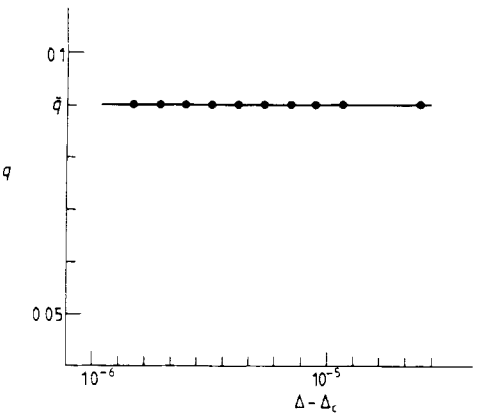

Figure 10. Wavevector q against $\Delta - \Delta_c$ if one approaches the point Q_1 from the modulated phase with $p = 3$, $k = 3$. $\tilde{q}$ is the resulting residual wavevector.

i.e. a first-order transition. This result clearly shows that Q_1 is not a Lifshitz point but a critical endpoint (see e.g. Kincaid and Cohen (1974)).

Denoting this residual wavevector by $\tilde{q}$ we can now ask the question if this is only true for the point Q_1 or if this behaviour extends over a finite range on the ferromagnetic-modulated transition.

We have investigated this by calculating the residual wavevector $\tilde{q}$, defined as the q obtained at $|\Delta - \Delta_c| = 10^{-4}$, along the transition line. Since at Q_1 this distance from the critical value of Δ already gives the correct $\tilde{q}$ up to our numerical accuracy (see figure 10) we have used this as a definition of $\tilde{q}$. We find that at $Q_2 = (T^*, \Delta^*)$ this residual wavevector vanishes like

$$\tilde{q} \sim (\Delta^* - \Delta)^x \qquad \text{with } x = 0.81 \tag{31}$$

for $p = 3$, $k = 3$ (cf figure 11), so that for $T < T^*$ we have a second-order transition

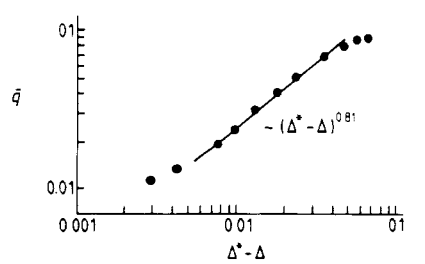

Figure 11. Log–log plot of the residual wavevector $\tilde{q}$ as a function of the asymmetry Δ along the ferromagnetic transition line ($p = 3$, $k = 3$).

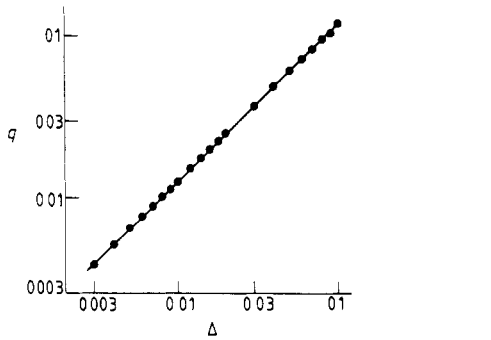

Figure 12. Log–log plot of the wavevector q against Δ ($\Delta_t = 0$) for $p = 4$, $k = 2$ ($T \to T_c = 1/\ln 3$). The slope is one.

as described already in § 6 while for $T > T^*$ the transition modulated-ferromagnetic is of first order. The critical point Q_2 was determined as $k_B T^*/J = 1.383$ and $\Delta^* = 0.145$ for $p = 3$ and $k = 3$. For $p = 3$ and $k = 2$ we have $k_B T^*/J = 0.95$ and $\Delta^* = 0.13$.

This situation is completely different for $p = 4$. There we find that indeed q vanishes at Q where the ferromagnetic and paramagnetic lines of stability touch at $\Delta = 0$ (see figure 5(d)). Furthermore, if one approaches the point from the modulated phase the exponent ζ is 1 (for $p = 4$, $k = 2$), see figure 12. Therefore, this point is really a Lifshitz point (Hornreich *et al* 1975, Michelson 1977). In addition on the whole line separating the modulated and the ferromagnetic phase we have a second-order transition. These results clearly indicate that the case with $p = 3$ is an exceptional one. Disregarding the simple case $p = 2$ (Ising) and $p = 3$, we find a Lifshitz point at $\Delta = 0$ for all other values of p and k and a second-order transition from the modulated to the ferromagnetic and paramagnetic phase.

8. Summary

We have studied the p-state asymmetric clock model on a Cayley tree with branching ratio k. Besides the ordered phases at low temperatures (ferromagnetic and helical phases) a modulated phase is found at finite asymmetry Δ. It is characterised by a continuously varying wavevector q in contrast to results for a similar model in mean field theory where q varies like a devil's staircase. For $p > 4$ and arbitrary k we found a Lifshitz point at zero asymmetry. The case $p = 3$ is an exceptional one for several reasons: firstly due to the crossing of the ferromagnetic and paramagnetic lines of stability there is a distinct point in the phase diagram at finite Δ but this point is not a Lifshitz point. Instead we find a whole range of first-order transition from the modulated into the ferromagnetic phase which is the second difference from the other cases. A very interesting feature that we find is that the exponent characterising the vanishing of the order parameter q at the second-order transition is not universal but depends on the asymmetry (or temperature). This point will be studied in detail in the future.

We have characterised the different phases of the model by the behaviour of the nonlinear map. Although this map shows bifurcations from one fixed point to a limit cycle there is no chaotic behaviour as found in maps arising in mean field theory of similar models. The main difference between the mean field maps and the map in this and related cases is the fact that here the maps are contracting towards the fixed point (and limit cycles) whereas in the other case the maps are area preserving (Hamiltonian). We note that on hierarchical lattices the study of nonlinear maps has also turned out to be very clarifying (Švrakić *et al* 1982, McKay *et al* 1982, Derrida *et al* 1983). We feel that the language of dynamical systems which we have used here will be a useful tool also in other areas.

Acknowledgments

We thank D Huse and W Selke for helpful comments. One of us (KF) acknowledges the hospitality at the Institut für Festkörperforschung of the KFA Jülich and CEN Saclay during the course of this work. The work at Los Alamos was performed under the auspices of USDOE.

References

Aubry S 1978 *Solitons and Condensed Matter Physics* ed A R Bishop and T Schneider (Berlin: Springer) p 264

Bak P 1981 *Phys. Rev. Lett.* **46** 791

Barber M N 1982 *J. Phys. A: Math. Gen.* **15** 915

Baumgärtel H G and Müller-Hartmann E 1982 *Z. Phys.* B **46** 227

Cardy J L 1982 *Nucl. Phys.* B **205** 17

Derrida B, Eckmann J P and Erzan A 1983 *J. Phys. A: Math. Gen.* **16** 893

Elliott R J 1961 *Phys. Rev.* **124** 346

Helleman R 1980 in *Fundamental Problems in Statistical Mechanics*, vol 5, ed EGD Cohen (Amsterdam: North-Holland) p 165

Hornreich R M, Luban M and Shtrikman S 1975 *Phys. Rev. Lett.* **35** 1678

Huse D A 1981 *Phys. Rev.* B **24** 5180

Jensen M H and Bak P 1983 *Phys. Rev.* B **27** 1683

Kardar M 1982 *Phys. Rev.* B **26** 2693

Kardar M and Berker A N 1982 *Phys. Rev. Lett.* **48** 1552

Kincaid J M and Cohen EGD 1974 *Phys. Lett.* **50A** 317

McKay S, Berker M N and Kirkpatrick S 1982 *Phys. Rev. Lett.* **48** 767

Michelson A 1977 *Phys. Rev.* B **16** 577, 585

Moraal H 1981 *Physica* **105A** 472

—— 1982 *Z. Phys.* B **45** 237

Müller-Hartmann E and Zittartz J 1974 *Phys. Rev. Lett.* **33** 893

Ostlund S 1981 *Phys. Rev.* B **24** 398

Öttinger H C 1982 *J. Phys. C: Solid State Phys.* **15** L1257

—— 1983 *J. Phys. C: Solid State Phys.* **16** L257

Selke W 1983 *Proc. Adv. Study Inst. on Modulated Struct. Mat. June 1983 Crete, Greece*

Selke W and Fisher M E 1979 *Phys. Rev.* B **20** 257

Selke W and Yeomans J M 1982 *Z. Phys.* B **46** 311

Švrakić N M, Kertész J and Selke W 1982 *J. Phys. A: Math. Gen.* **15** L427

Vannimenus J 1981 *Z. Phys.* B **43** 141

Yeomans J M and Fisher M E 1981 *J. Phys. C: Solid State Phys.* **14** L835